JCTC Journal of Chemical Theory and Computation

Density Functional and Basis Set Dependence of Hydrated Ln(III) Properties

Aurora E. Clark*

Department of Chemistry, Washington State University, P.O. Box 644630, Pullman, Washington 99164

Received November 20, 2007

Abstract: Benchmark studies of $Ln(H_2O)_{1,8-9}^{3+}$ (Ln = La, Lu) have been performed to assess the calculated properties obtained with local density approximation, generalized gradient approximation (GGA), meta-GGA, and hybrid functionals, when used with small- and large-core relativistic effective core potentials and their associated bases. Basis set dependence and the importance of specific functions to adequately describe the Ln atomic orbitals have been determined. The lanthanide contraction has been found to be an insufficient metric for characterizing the quality of a method/basis set combination due to cancellation of the errors. The electrostatic description obtained by natural population analysis has been examined, and an alternative partitioning of the valence space, which includes the 6s6p5d4f natural atomic orbitals, has been proposed.

Introduction

The aqueous chemistry of metal ions has an immense amount of literature available due to its fundamental importance in a variety of areas including biological systems, metal coordination, complexation behavior, and so forth. In the absence of metal-binding ligands, water molecules will coordinate to the metal to form the inner coordination shell. Within the alkali and alkaline earth series, the metal−water interaction is exclusively ionic in character.[1,2] In contrast, transition metal aquo complexes have coordination geometries that are strongly dependent upon the metal electronic state due to the participation of the d orbitals in the $M-OH_2$ bond.[3] Between these bonding extremes lie the lanthanide (Ln) and actinide (An) elements, whose f and d orbitals may participate in bonding with ligating water, but in a manner that is dependent upon the position of the element within the period and its oxidation state. In general, earlier An and Ln may have $M-OH_2$ interactions with some covalent character, while later in the series the interactions become more ionic.[4]

The solution chemistry of trivalent Ln has relevance to environmental remediation and the terrestrial migration of fission products at United States Department of Energy nuclear weapons facilities like the Hanford site. The potential closure of the nuclear fuel cycle currently proposes liquid/liquid extraction techniques for separating both 4f and 5f elements, mandating a fundamental understanding of the multiscale solution behavior of Ln and An. Using X-ray, extended X-ray absorption fine structure, and neutron diffraction methods, present experimental capabilities are able to determine bond lengths and angles that constitute molecular-scale solution geometry in a single phase from averaged ensembles, while long-range solvent organization is inferred from the bulk. Structural information within intermediate-length scales is experimentally formidable because it is buried in the bulk response of the condensed state. Owing to such experimental limitations, computational chemistry is a necessary complement to predict the molecular- and mesoscale solution behavior of f elements. Density functional theory (DFT) has been used for some time to calculate geometries and electronic structure of strongly bound Ln(III) complexes. Within that literature, it has been established that relativistic effective core potentials (RECPs) can capture the relativistic effects from all electron scalar-relativistic Douglas−Kroll−Hess calculations.[5] The relativistic effects upon the Ln−X bond lengths and the calculated Ln contraction have also been examined.[6–8] Both large- and small-core RECPs (and their associated basis sets) have been developed for Ln and are often used interchangeably, with little discussion of the influence of the f electrons upon electrostatic properties,

* Author e-mail: auclark@wsu.edu.

10.1021/ct700317p CCC: $40.75
Published on Web 04/05/2008

bonding, or the importance of basis sets upon calculated geometric and electronic structures. Comparisons of small- and large-core RECP[9,10] geometries do reveal longer Ln−X bond lengths from large-core calculations, presumably because of poorer treatment of the core-valence correlation relative to the small-core RECP. The extent to which the 4f electrons participate in bonding is a topic of current debate within the literature. While most studies indicate that the 4f orbitals/electrons do not participate in bonding, some systems (e.g., lanthanide trihalides) have shown pronounced 4f hybridization indicative of bonding interactions.[6]

In contrast to "strongly" bound Ln(III) complexes, the inner coordination sphere of aqueous Ln(III) is known to be dynamic, with significant exchange of the first- and second-shell H_2O being possible.[4] Lanthanides early in the series are predominantly nine-coordinate (nona-aqua) in solution, while late lanthanides have a propensity for being eight-coordinate (octa-aqua). Given the relative "weakness" of the $Ln-OH_2$ interaction, it is imperative that systematic benchmarks are performed to elucidate the most appropriate functionals, basis sets, and electronic structure analysis methods to be used. Indeed, such benchmarks may help elucidate patterns in geometric and electronic structure within the computational chemistry literature of strongly bound Ln systems. To this end, we have determined and analyzed the optimal geometric and electronic structures of $Ln(H_2O)_{1,8-9}^{3+}$ (Ln = La, Lu), using either local density approximation (LDA), generalized gradient approximation (GGA), meta-GGA, or hybrid density functionals in combination with small- and large-core RECPS and their associated contracted and uncontracted basis sets. A detailed analysis of the atomic orbital (AO) coefficients and atomic energies of Ln^{3+} cations has revealed specific functions necessary for describing the Ln AOs. Natural population analyses[11] with different partitioning of the core/valence/Rydberg natural atomic orbitals (NAOs) have also been studied, and a modified partitioning scheme has been proposed for calculating the Ln(III) charges. This series of molecules has been chosen due to their closed-shell electronic configurations, which allows for the basis set, density functionals, and RECPs to be examined in the absence of any errors associated with first-order spin–orbit coupling.

Computational Methods

The optimized structures of $Ln(H_2O)_{1,8-9}^{3+}$ (Ln = La, Lu) were obtained using local spin density approximation (LSDA; SVWN5 and the modern equivalent SPW92),[12–16] GGA (PBE, PW91, and B88P86),[17–22] hybrid (B3LYP and PBE0),[23–26] and meta-GGA functionals (TPSS).[27] These calculations were performed in NWChem[28] and Gaussian03.[29] The former employed a self-consistent field (SCF) energy convergence criterion of 10^{-6}, an integral internal screening threshold of 10^{-16}, a numerical integration grid of 10^{-8}, and a tolerance in Schwarz screening for the Coulomb integrals of 10^{-12}. Gaussian03 calculations used the Ultrafine integration grid (99 590 points), and SCF convergence was set to "verytight" (10^{-6}). "Verytight" optimization convergence was not used in all cases due to computational expense. In test cases, differences in energy between the default and "verytight" optimization criteria were less than 1.6 millihartrees. All geometries were confirmed to be local minima, with no imaginary vibrations unless otherwise noted. Both small-core Stuttgart−Dresden (SD) RECP[30,31] (which includes the $n = 4$–6 shells in the valence space) and large-core SD RECP[32] (which includes the $n = 5$ and 6 shells in the valence space) were examined with their associated generally contracted, segmented contracted, and uncontracted basis sets. The oxygen and hydrogen atoms were treated with an aug-cc-PVDZ basis set.[33] Natural population[11] and Mulliken population[34] analyses were performed at the optimized geometries. All calculations were performed on the massively parallel Linux cluster in the Molecular Science Computing Facility in the William R. Wiley Environmental Molecular Sciences Laboratory at the Pacific Northwest National Laboratory, or at the National Energy Research Scientific Computing Center (NERSC), a DOE Office of Science user facility at Lawrence Berkely National Laboratory.

Results and Discussion

It is well-known that the lanthanide series exhibits a pronounced decrease in the ionic radii with increasing atomic number.[35] Filling the 4f orbitals improves shielding of the nuclear charge and is most pronounced early in the series. Subsequently, the decrease in ionic radii is larger at the beginning of the series than at the end. This trend may be monitored by examining the monotonic decrease of Ln−X bond lengths (X = Lewis-base donor), wherein a quadratic dependence across the series has been observed. This behavior is observed in X-ray structures of isostructural Ln complexes[36,37] (Ln = La–Lu), in addition to more limited sets of solid-state materials[38,39] and coordination compounds.[40,41] Quadrelli suggested that individual classes of bond lengths can be fit by a second-order polynomial.[36] More recent studies by Seitz et al.[37] have indicated that the ligand field responds to a change in the average metal ion size to distribute the metal–ligand bond-length changes; however, taking the average bond length does show the anticipated contraction. There, it was pointed out that the quadratic dependence of the lanthanide contraction can be derived from the model proposed by Slater[42] and later modified by others.[43,44] This model utilizes empirical rules for the shielding of the nuclear charge Z from electrons in a particular orbital by inner electron shells, expressed by a screening constant s.

The lanthanide contraction has been calculated by Pyykko[45] and others through the comparison of the difference of the ionic radii of lanthanum and lutetium, as measured by bond length Ln−X for isostructural species:

$$\Delta_{Ln} = r_e(LaX) - r_e(LuX)$$

Experimentally and theoretically, the Ln contraction has been found to be dependent upon the coordination number, the charge of the ions, and, some have suggested, bond type. Generally, large contractions are observed for soft bonds and small contractions are observed for stiffer ones.[46] Importantly, the calculated Δ_{Ln} is often used as a metric for assessing the reliability and quality of an *ab initio* calculation.

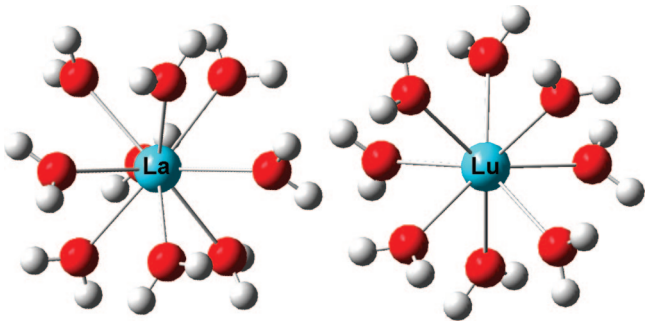

Figure 1. DFT-optimized tricapped trigonal bipyramidal $La(H_2O)_9^{3+}$ and square antiprismatic structure of $Lu(H_2O)_8^{3+}$. Specific geometric parameters are presented in Tables 1 and 2.

This is problematic, as computationally important errors within calculations on La and Lu may cancel when determining the contraction. Here, we use a variety of metrics to assess the quality of particular method/basis set combinations, illustrating the potential pitfalls of relying on computed lanthanide contraction values.

Geometric Dependence Upon RECP and Basis. *Small-Core RECP and Segmented Contracted Basis.* Two small-core RECPs (28 e^- in the core) and basis sets are available for La^0 and Lu^0 from the Stuttgart group. The first basis set to be considered is the (14s13p10d8f6g)/[10s8p5d4f3g], which is based upon a segmented contraction scheme.[31] Here, the most diffuse s function, which has an exponent of 0.02 in La^0 and 0.03 in Lu^0, has been removed to yield a [9s8p5d4f3g] contracted Gaussian basis, so as to prevent linear dependence errors. The performance of the (13s13p10d8f6g)/[9s8p5d4f3g] basis was first examined by B3LYP optimization of $La(H_2O)_9^{3+}$ and $Lu(H_2O)_8^{3+}$ in the gas phase and subsequent comparison with available experimental data. As seen in Figure 1, the nona-aqua La(III) adopts a tricapped trigonal bipyramidal structure, while the octa-aqua Lu(III) adopts a square antiprismatic arrangement of the ligating waters. X-ray structures in dilute $LaCl_3$ solutions observe an average nona-aqua La−OH_2 bond distance of 2.580 Å, while dilute $LuCl_3$ solutions have average octa-aqua Lu−OH_2 distances of 2.338 Å.[47,48] This compares well (within 0.03 Å) with the average calculated B3LYP values of $r_{La-OH_2} = 2.618$ Å and $r_{Lu-OH_2} = 2.369$ Å. IR data are also available for dilute solutions of $[Ln(H_2O)_{9-8}^{3+}]$ $(C_2H_5SO_4)_3$ wherein the Ln−OH_2 stretch for $La(H_2O)_9^{3+}$ occurs at 316 cm^{-1} and, for $Lu(H_2O)_8^{3+}$, at 342 cm^{-1}.[49] B3LYP calculates these stretches to be at 279 and 329 cm^{-1} (unscaled), respectively (Table 1). These low vibrational frequencies are consistent with the somewhat too long Ln−OH_2 bond lengths.

To examine the lanthanide contraction, Δ_{Ln}, the Ln−OH_2 bond lengths for isostructures $La(H_2O)_8^{3+}$ and $Lu(H_2O)_8^{3+}$ were compared (Figure 1 and Table 1). The calculated lanthanide contraction for these hydrates is 0.215 Å, in excellent agreement (±0.005 Å) with four-component relativistic Hartree−Fock (HF; DHF) and MP2 (RMP2) calculations of $Ln(H_2O)^{3+}$.[50] Given previous observations regarding the sensitivity of the lanthanide contraction to the coordination number and type of ligands, we sought to directly compare the DHF and RMP2 values with B3LYP by calculating the optimized geometries of $La(H_2O)^{3+}$ and $Lu(H_2O)^{3+}$. Here, the hybrid functional predicts $r_{La-OH_2} = 2.289$ Å and $r_{Lu-OH_2} = 2.094$ Å. This compares to reported DHF values of 2.34 and 2.13 Å, respectively, and RMP2 values of 2.29 and 2.08 Å, respectively. Thus, there is clearly excellent agreement between B3LYP (using a RECP basis) and RMP2 for individual bond lengths, and all three methods yield lanthanide contraction values that deviate by only 0.01 Å from each other.

The number of valence functions within the contracted segmented set is quite large, particularly when compared to the small-core contracted basis sets for An that are routinely used (12s11p10d8f)/[8s7p5d4f] and truncated to [6s6p5d3f].[51,52] Consequently, the importance of the most diffuse functions to the total electronic energy, geometry, IR frequencies, and lanthanide contractions of isostructural $La(H_2O)_8^{3+}$ and $Lu(H_2O)_8^{3+}$ was examined. The most diffuse functions from each shell were first systematically removed and the single-point energies calculated at the optimized [9s8p5d4f3g] geometries. The energy differences between the original and truncated bases are indicative of the contribution of the omitted basis to the total electronic energy. The geometry was then reoptimized using the truncated basis to determine the importance of the omitted functions to structural parameters and the frequency of the IR-active totally symmetric Ln−OH_2 stretch, ν_{Ln-H_2O} (Table 1).

The first truncated basis omits the three g functions to yield the [9s8p5d4f] set. The energetic consequence of the g functions is minor, as the total electronic energy from the single-point calculation is increased by only 1.6 and 2.4 millihartrees for octa-aqua La(III) and Lu(III), respectively. The optimization of $Ln(H_2O)_8^{3+}$ with the [9s8p5d4f] basis yields nearly identical geometries and vibrational frequencies to those obtained with [9s8p5d4f3g]. Omission of the most diffuse f function, which has an exponent of 0.1973 for La^0, increases the single-point energy of $La(H_2O)_8^{3+}$ by 3.4 millihartrees, and subsequent geometry optimization implies minimal impact on the structure and IR spectra. Yet, removal of the most diffuse f function on Lu^{3+} (exponent of 0.4244) increases the single-point electronic energy of $Lu(H_2O)_8^{3+}$ by 108.7 millihartrees in the [9s8p5d3f] basis. Subsequently, geometry optimization decreases the Lu−OH_2 bond length by 0.05 Å and shifts the frequency of the symmetric stretch, ν_{Lu-OH_2}, by 30 cm^{-1} relative to that calculated in the larger [9s8p5d4f] basis. Truncating the most diffuse p function for La^0 and Lu^0 (with a 0.08 exponent), to yield the [9s7p5d43f] basis, alters the single-point electronic energies by less than 1.6 millihartrees and has negligible structural consequences. However, removing the second most diffuse p functions with exponents of 0.2292 and 0.2858 on La^0 and Lu^0, respectively, increases the energy by 63.4 and 38.9 millihartrees. The net affect after geometry optimization in the [9s6p5d3f] basis is a contraction of r_{La-OH_2} by 0.06 Å and a 50 cm^{-1} shift in ν_{La-OH_2} in $La(H_2O)_8^{3+}$, and a 0.03 Å bond-length shortening in $Lu(H_2O)_8^{3+}$ with a 30 cm^{-1} shift in ν_{Lu-OH_2}. Turning to the s functions, we observe that truncating the most diffuse s, with exponents of 0.0467 and 0.079 on La^0 and Lu^0, has little affect upon the energy (<1.5 millihartree) or geometry; however, omission of the functions with La^0 and Lu^0

Table 1. C_1 B3LYP Structural Parameters and the Symmetric Ln−OH_2 Vibrational Stretching Frequency (cm^{-1}), ν_{Ln-OH_2}, Obtained for $La(H_2O)_{8-9}^{3+}$ and $Lu(H_2O)_8^{3+}$ as a Function of General (ano) and Segmented (seg) Contracted Metal Basis Sets Using Both Small-Core (ECP28MWB) and Large-Core (ECP47MWB for La^{3+}, ECP60MWB for Lu^{3+}) RECPs[a]

	~symm	tol	$<r_{M-O}>$	$\theta_{O1-M-O2}$	ν_{Ln-OH_2}[b,c]	E	$<\Delta Ln>$
			$La(H_2O)_9^{3+}$				
ECP28MWB							
[9s8p5d4f3g] seg	C_3	0.01	2.618	69.7	279	−1122.987628	
[9s8p5d3f] seg	C_3	0.01	2.620	69.8	280	−1122.981900	
			$La(H_2O)_8^{3+}$				
ECP28MWB							
[6s6p5d4f3g] ano	S_8, C_4, C_2	0.010	2.580	78.0	293	−1046.505984	0.212
[9s8p5d4f3g] seg	S_8, C_4, C_2	0.010	2.580	78.0	293	−1046.507198	0.215
[9s8p5d4f] seg	S_8, C_4, C_2	0.010	2.582	78.0	293	−1046.504786	0.213
[9s8p5d3f] seg	S_8, C_4, C_2	0.010	2.581	78.0	294	−1046.501456	0.254
[9s7p5d3f] seg	S_8, C_4, C_2	0.010	2.581	78.0	294	−1046.501092	0.255
[9s6p5d3f] seg	C_4, C_2	0.001	2.525	76.6	342	−1046.441367	0.223
[8s6p5d3f] seg	C_4, C_2	0.001	2.524	76.6	342	−1046.440913	0.224
[7s6p5d3f] seg	C_4	0.001	2.506	74.9	358	−1046.417898	0.240
[6s6p5d3f] seg	S_8, C_4, C_2	0.010	2.332	69.4	565	−1046.055109	0.275
ECP47MWB							
[5s4p3d]	S_8, C_4, C_2	0.010	2.603	78.0	288	−642.433080	0.213
			$Lu(H_2O)_8^{3+}$				
ECP28MWB							
[6s6p5d4f3g] ano	S_8, C_4, C_2	0.100	2.369	77.9	328	−1847.144368	
[9s8p5d4f3g] seg	S_8, C_4, C_2	0.100	2.365	77.8	329	−1847.129760	
[9s8p5d4f] seg	C_2	0.010	2.369	77.9	329	−1847.128037	
[9s8p5d3f] seg	S_8, C_4, C_2	0.010	2.327	78.0	353	−1847.021075	
[9s7p5d3f] seg	S_8, C_4, C_2	0.010	2.326	78.0	354	−1847.020175	
[9s6p5d3f] seg	S_8, C_4, C_2	0.010	2.301	77.6	384	−1846.985048	
[8s6p5d3f] seg	S_8, C_4, C_2	0.010	2.300	77.6	385	−1846.984341	
[7s6p5d3f] seg	C_2	0.001	2.266	75.1	436	−1846.926420	
[6s6p5d3f] seg	C_1		2.057	73.0	629	−846.201021	
ECP60MWB							
[5s4p3d]	S_8, C_4, C_2	0.010	2.390	77.9	322	−650.797635	

[a] Nearest symmetry group (symm), tolerance to reach higher symmetry (tol), average bond lengths ($<r_{M-O}>$ in Å), maximum deviation from the average bond lengths (Δr_{M-O}^{max} in Å), bond angles ($\theta_{O1-M-O2}$ in deg), total electronic energies (E in hartrees), and average Ln contraction ($<\Delta Ln>$ in Å) are presented. [b] Experimental value = 316 cm^{-1}, ref 49. [c] Experimental value = 342 cm^{-1}, ref 49.

exponents of 0.2539 and 0.4408 increases the energy by up to 82.9 millihartree. Similar to the above observations, removal of the second most diffuse s function shortens the metal–ligand bond lengths by ~0.04 Å and increases the energy of the symmetric metal−water vibrational stretch by ~50 cm^{-1}. Completely unrealistic energies, geometries, and frequencies are obtained with the [6s6p5d3f] basis.

Despite the dramatic changes that occur in geometry when using these truncated basis sets, it is quite interesting to note that the value of lanthanide contraction is relatively constant. Indeed, Δ_{Ln} varies by only 0.025 Å between the [9s8p5d4f3g] and [7s6p5d3f] bases, clearly indicating that the lanthanide contraction is a poor metric for assessing the quality of geometries of lanthanide complexes. When these structural and vibrational data are compared as a function of the basis with available experimental data, the closest agreement for $Lu(H_2O)_8^{3+}$ occurs with the [9s8p5d3f] and [9s7p5d3f] basis sets. Since the largest basis set does not yield the closest geometric parameters relative to experimental results, there are obvious methodological errors associated with using the B3LYP functional (*vide infra*). However, a second solvation shell may also improve the agreement with experimental structures and frequencies, creating more consistency in the accuracy of the various basis sets. While it might be tempting to assume that the same truncated basis sets that perform well for octa-aqua Lu(III) would yield similar quality results for nona-aqua La(III), geometry optimization of $La(H_2O)_9^{3+}$ with either the [9s8p5d3f] or [9s7p5d3f] basis sets yields structures that deviate farther from experiment than that obtained with the [9s8p5d4f] basis (Table 1). As a consequence of the energetic and geometric observations as a function of the basis, those bases smaller than [9s8p5d4f] are not recommended for use when studying the solvation properties of Ln(III).

This brings up the question, however, of why the truncated basis sets perform so badly. Contraction errors and inflexibility of the basis may be responsible, or perhaps the truncated functions are genuinely necessary for an accurate description of the Ln atomic orbitals. Intertwined is the fact that DFT functionals incorporate some amount of correlation energy, which may itself lead to deviations in the treatment of contracted and uncontracted bases, and it is further possible that the DFT density may be significantly different from the Hartree−Fock (HF) density for which the basis set was developed. To explore these issues, the total electronic energies and AO coefficients of La^{3+} and Lu^{3+} cations were systematically examined using HF, a single SCF cycle of DFT fixed at the HF density, and SCF-optimized DFT. Both the segmented contracted and uncontracted bases were investigated, and we define the difference in energy between the two bases as the contraction error:

$$\Delta E_{cont} = E_{contracted} - E_{uncontracted}$$

Table 2. Structural Parameters and the Symmetric Ln−OH_2 Vibrational Stretching Frequency (cm^{-1}), ν_{Ln-OH_2}, of $Ln(H_2O)_{8-9}^{3+}$ (Ln = La, Lu) Obtained with LDA, GGA, and meta-GGA Functionals Using the Small-Core RECP and the [9s8p5d4f3g] Segmented Basis[a]

method	~symm	tol	$<r_{M-O}>$	$\theta_{O1-M-O2}$	ν_{Ln-OH_2}	$<\Delta Ln>$
			$La(H_2O)_9^{3+}$			
TPSS	C_3	0.01	2.600	69.8	280	
B3LYP	C_3	0.01	2.618	69.7	279	
			$La(H_2O)_8^{3+}$			
SVWN5	S_8, C_4, C_2	0.010	2.496	78.0	326	0.213
SPW92[b]	C_2	0.001	2.496	78.0	321	0.213
PW91	S_8, C_4, C_2	0.010	2.564	77.9	294	0.208
B88P86	S_8, C_4, C_2	0.010	2.569	78.0	291	0.209
PBE	S_8, C_4, C_2	0.010	2.569	78.0	292	0.207
TPSS	S_8, C_4, C_2	0.010	2.565	78.0	294	0.214
B3LYP	S_8, C_4, C_2	0.010	2.580	78.0	293	0.215
PBE0	S_8, C_4, C_2	0.010	2.556	77.8	300	0.191
			$Lu(H_2O)_8^{3+}$			
SVWN5	C_2	0.010	2.283	77.5	368	
SPW92	C_4, C_2	0.010	2.283	77.7	351	
PW91	S_8, C_4, C_2	0.010	2.356	77.8	328	
B88P86	S_8, C_4, C_2	0.010	2.360	77.9	325	
PBE	S_8, C_4, C_2	0.010	2.361	77.8	325	
TPSS	S_8, C_4, C_2	0.010	2.351	77.6	327	
B3LYP	S_8, C_4, C_2	0.100	2.365	77.8	329	
PBE0	S_8, C_4, C_2	0.100	2.365	77.8	322	

[a] Nearest symmetry group (symm), tolerance to reach higher symmetry (tol), average bond lengths ($<r_{M-O}>$ in Å), maximum deviation from the average bond lengths (Δr_{M-O}^{max} in Å), bond angles ($\theta_{O1-M-O2}$ in deg), total electronic energies (Hartree), and average Ln contraction ($<\Delta Ln>$ in Å) are presented. [b] Optimized structure had a single imaginary vibration at −33 cm^{-1}.

Using HF, ΔE_{cont} values for the [9s8p5d4f3g] segmented basis of La^{3+} and Lu^{3+} are 0.34 and 4.51 millihartrees, respectively. B3LYP performed at the HF density with a single SCF cycle yields contraction errors for La^{3+} and Lu^{3+} of 0.24 and 1.16 millihartrees, indicating that the intrinsic correlation obtained by B3LYP should not affect basis set performance relative to HF. In contrast, the correlation error obtained from the SCF-optimized B3LYP energies of La^{3+} and Lu^{3+} are 0.66 and 24.0 millihartrees, respectively. This indicates that, while the B3LYP density for La^{3+} is quite similar to that of HF, it is significantly different for Lu^{3+}. These numerical results are shown pictorially in Figure 2, along with plots of the uncontracted HF density, ρ_{HF}, and the B3LYP difference densities ($\rho_{HF} - \rho_{B3LYP}$) for La^{3+} and Lu^{3+}. In the case of La^{3+}, B3LYP and HF both calculate the same density, and thus ($\rho_{HF} - \rho_{B3LYP}$) is negligible everywhere (Figure 2a). However, for Lu^{3+}, it is clear that the B3LYP density deviates significantly relative to that obtained by HF (Figure 2b). Thus, the large contraction error obtained from the B3LYP calculation on Lu^{3+} (Figure 2, right-hand panel) arises from the fact that the DFT density using the contracted basis is very similar to that of HF, while uncontracting the basis leads to a different density and energy (Figure 2b).

Comparison of the HF and B3LYP SCF AO coefficients for Lu^{3+} indicates that, in general, the more diffuse basis functions have larger contributions to the occupied AOs in B3LYP than in HF, which leads to the density difference shown in Figure 2b. Monitoring the HF and B3LYP energies for Lu^{3+} with the uncontracted segmented basis as a function of truncation level reveals significant changes when specific functions are removed from the basis, indicating that HF calculations will experience the same basis set dependence as B3LYP. The energetically crucial functions are the 10th to 12th s, having exponents of 0.4408, 1.0287, and 2.6778, respectively, and the 12th p in the (13s13p10d8f6g), which has an exponent of 0.2858. This is the same behavior observed in $Lu(H_2O)_8^{3+}$, illustrating that these functions are crucial for the correct description of the atomic orbitals of Lu(III). The HF and B3LYP SCF AO coefficients show that these functions help describe the 4s, 5s, and 5p AOs within the $[Ar]4s^23d^{10}4p^65s^24d^{10}5p^64f^{14}$ electronic configuration of Lu^{3+}, where the $[Ar]3d^{10}$ electrons are in-core. Interestingly, the most diffuse uncontracted f function (with an exponent of 0.4244) has a significant energetic consequence, yet it participates only in the unoccupied f atomic orbitals. The importance of diffuse functions is not necessarily surprising, as such functions are likely needed to describe its filled 4f shell. Monitoring the total HF and B3LYP electronic energies for La^{3+} ($[Ar]4s^23d^{10}4p^65s^24d^{10}5p^6$ electronic configuration) using the uncontracted basis as a function of truncation reveals significant changes to both the HF and B3LYP energies when the p function with an exponent of 0.2292 is removed (the ninth p in the (13s13p10d8f6g) set), and similarly when the s functions with 0.5672 and 0.2539 exponents are removed (the 11th and 12th s functions in the (13s13p10d8f6g) set, respectively). The SCF basis function coefficients indicate that the 11th s function contributes to the 4s and 5s AOs, while the 12th s function has large coefficients for the 5s AO, and the ninth p function contributes to the 4p and 5p AOs. On the basis of these results, it is clear that truncating the Stuttgart small-core basis set amounts to removing key functions necessary to describe the Ln atomic orbitals.

Small-Core RECP and General Contracted Basis. The second basis set to be considered is the (14s13p10d8f6g)/[6s6p5d4f3g] atomic natural orbital basis set, which is based upon a generalized contraction scheme.[29] These geometries (Table 1) are found to be nearly identical to those obtained by the segmented [9s8p5d4f3g]. The agreement between the two bases is slightly better in $La(H_2O)_8^{3+}$ (r_{La-OH_2} deviations of 0.0001 Å) than in $Lu(H_2O)_8^{3+}$ (r_{Lu-OH_2} deviations of 0.003 Å). This result is not entirely unanticipated, as the B3LYP La^{3+} and Lu^{3+} cation densities are nearly identical using either the uncontracted segmented or generalized contracted natural orbital basis.

Large-Core RECP and Basis. Previous calculations[9] utilizing large-core RECPs for Ln have noted that placement of the f electrons and orbitals in the core leads to qualitatively similar structural parameters, but with increased bond lengths. This is presumably due to poorer treatment of core−valence correlation relative to the small-core RECPs. The large-core Stuttgart RECP for La^{3+} places the $[Kr]4d^{10}$ electrons in the core, leaving $5s^25p^6$ in the valence space. Geometry optimization of $La(H_2O)_8^{3+}$ yields a square antiprismatic structure near S_8 symmetry, similar to those found using the two small-core RECPs. The average La−OH_2 bond length is 2.603 Å, which is 0.023 Å longer than the small-core bond lengths using the (13s13p10d8f6g)/[9s8p5d4f3g] segmented

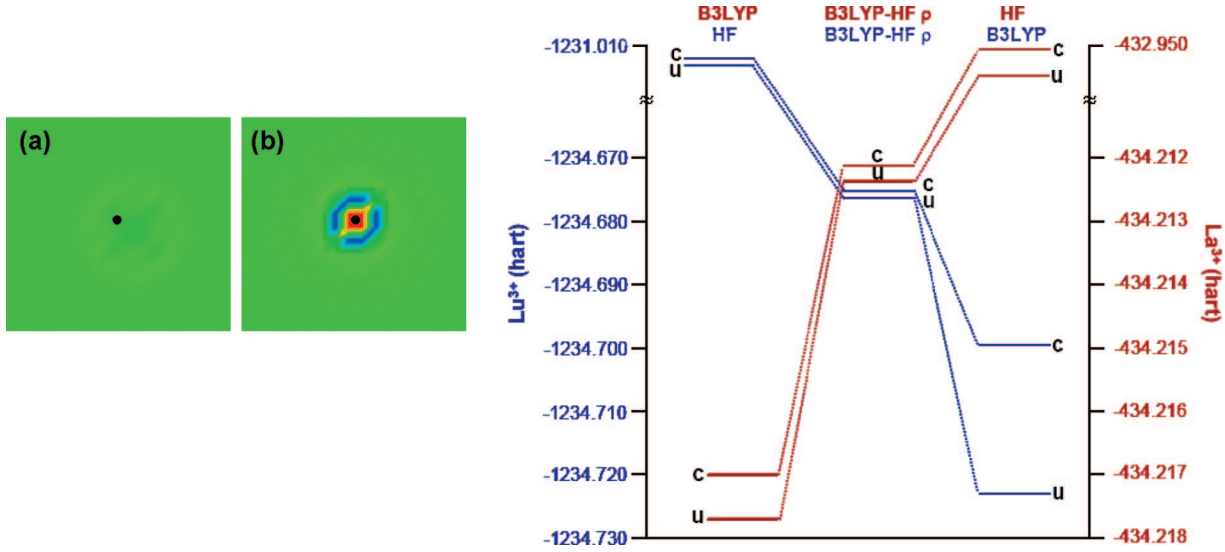

Figure 2. Left-hand panel: the difference density between HF and B3LYP ($\rho_{HF} - \rho_{B3LYP}$) for (a) La^{3+} and (b) Lu^{3+} using the uncontracted small-core [9s8p5d4f3g] basis [scale of the density difference: -6.79×10^{-2} (blue), 7.23×10^{-2} (red)]. Right-hand panel: the total electronic energies of La^{3+} (red) and Lu^{3+} (blue) with HF, B3LYP fixed at the HF density, and fully SCF-optimized B3LYP using the small-core [9s8p5d4f3g] contracted (c) and uncontracted (u) basis sets.

and (14s13p10d8f6g)/[6s6p5d4f3g] general contracted basis sets, respectively. The total number of H bonds present in $La(H_2O)_8^{3+}$ is the same in all three cases; however, the large-core basis also increases the average H-bond length from ~2.958 Å in the small-core calculations to 2.986 Å. Similar results are obtained for $Lu(H_2O)_8^{3+}$, wherein the Lu−OH_2 bond length increases by 0.025 Å and the average H-bond length for the 16 hydrogen bonds increases by 0.032 Å relative to the small-core (13s13p10d8f6g)/[9s8p5d4f3g] segmented calculation. This is important, as it indicates that the large-core RECP affects not only the immediate Ln−X bond length but also structural features that extend beyond the metal's nearest bonding interactions. Interestingly, the perturbations in hydrogen bonding as a function of RECP are not attributable to differences in the electrostatic interactions, as both Mulliken[34] and NPA[11] charges are virtually unchanged (*vide infra*).

Geometric Dependence Upon Density Functionals. The Jacob's ladder of density functionals[53] describes the relative increase in the ability of approximate exchange and correlation functionals, E_{XC}'s, to approach the density given by the exact many-body wave function. Depending on the level of covalency within the metal–ligand bond, LDA, GGA, meta-GGA, and hybrid functionals can give quite different electronic and geometric descriptions for f-element complexes.[54] Using LDA with spin–orbit corrections on lanthanide atoms has been shown to yield ionization potentials close to experimental values,[55] yet the electronic description becomes less accurate in molecular calculations, and overbinding is often predicted.[56,57]A variety of GGA functionals (BLYP, BP, BPW, and PWPW) have been successful in describing LnX_3 compounds (X = F, Cl, Br, I; Ln = La, Gd, Lu),[55] utilizing the RECPs and basis sets of Cundari and Stevens.[58,59] Some studies have shown that hybrid functionals predict significantly longer bond lengths than GGA functionals,[54] yet B3LYP is often the functional of choice within computational lanthanide chemistry, and very successful studies have been performed.[9] In order to assess the applicability of different approximate exchange correlation functionals to describe hydrated Ln(III), we have examined the geometries and lanthanide contraction values of isostructural $La(H_2O)_8^{3+}$ and $Lu(H_2O)_8^{3+}$ using LSDA, GGA, meta-GGA, and hybrid functionals with the small-core RECP and the [9s8p5d4f3g] segmented basis (Table 2).

In general, each density functional predicts similar square antiprismatic geometries for $Ln(H_2O)_8^{3+}$. Most have a high degree of symmetry and are near S_8, though $Lu(H_2O)_8^{3+}$ is typically less symmetric than $La(H_2O)_8^{3+}$. For the sake of comparison to experimental data, the functional performance for $Lu(H_2O)_8^{3+}$ will first be discussed. Recall that, experimentally, $r_{Lu-OH_2} = 2.338$ Å and $\nu_{Lu-OH_2} = 342$ cm^{-1}. Given prior observations of overbinding in LDA,[56,57] it is not surprising that LSDA predicts the shortest metal–ligand bond lengths, $r_{Lu-OH_2} = 2.283$ Å. Interestingly, its calculated frequency for the symmetric metal–ligand stretch shifts by 17 cm^{-1}, depending upon the functional, with SPW92 predicting the closest value, $\nu_{Ln-OH_2} = 351$ cm^{-1}, relative to experimental results. Within the GGA functionals, PW91 yields metal–ligand bond lengths that are ~0.04 Å shorter than those of B88P86 and PBE; yet, each GGA predicts very close ν_{Ln-OH_2} values ($\nu_{Ln-OH_2} = 325-328$ cm^{-1}). The meta-GGA TPSS functional agrees most closely with the experimental average Lu−OH_2 distance (within 0.013 Å); however, its calculated frequency for the symmetric metal–ligand stretch is comparable to the GGA and hybrid functionals, all of which predict too low of a value by ~20 cm^{-1}. The hybrid B3LYP and PBE0 functionals predict the longest r_{Lu-OH_2} values, overestimating the distance by 0.03 Å.

Additionally, some of the trends in structure for $Lu(H_2O)_8^{3+}$ do not hold for the octa-aqua La(III) complex. For example, there is a 0.02 Å deviation in the La−OH_2 bond length between the B3LYP and PBE0 hybrid functionals in $La(H_2O)_8^{3+}$, while the calculated Lu−OH_2 bond

lengths for the same functionals are essentially identical. Indeed, the hybrid PBE0 functional yields a metal–ligand bond length for $La(H_2O)_8^{3+}$ that is much closer to that predicted by TPSS than that by B3LYP. Examining the isostructural octa-aqua species allows for investigation of the functional dependence of the calculated lanthanide contraction values. LSDA, TPSS, and B3LYP predict essentially the same Δ_{Ln} of 0.21 Å, while the GGA and PBE0 functionals predict somewhat shorter values. This again highlights the misleading nature of the lanthanide contraction as a metric for assessing the appropriateness of a given method, as techniques with nearly identical Δ_{Ln} values may have quite different individual metal–ligand bond lengths that may or may not agree well with experimental values. Given the good performance of the TPSS functional for $Lu(H_2O)_8^{3+}$, the structure of nona-aqua La(III) was optimized and those results compared to experimental ones (Table 2). Indeed, TPSS does yield slightly better agreement with the X-ray average r_{La-OH_2} than B3LYP (by 0.01 Å), yet it has essentially the same predicted frequency for the totally symmetric La−water stretch, which is nearly 40 cm^{-1} below the reported value.[49] It thus appears that no functional performs equally well for calculated bond lengths as for IR frequencies in the hydrated species with a single solvent shell. Some improvement may be expected upon increasing the basis set on the water ligands, or by adding a second solvation shell. Another experimental observable of interest to be compared is the free energy of hydration for Ln(III). That topic is beyond the scope of this paper, as it is also highly dependent upon the solvation models used; however, it is the topic of another manuscript.[60]

Population Analyses. Population analyses are a common way to characterize the electronic structure of metal atoms. Often, the large basis sets needed to describe d- and f-block metals makes standard Mulliken[34] and Löwdin[61] methods nonoptimal. Natural population analysis[11] (NPA) has emerged as one of the methods of choice for such systems because its partitioning of the orbital space decreases basis set dependence. NPA divides the molecular charge into atomic components in analogy to Löwdin's method,[61] where an occupancy-weighted symmetric (Löwdin) transformation is used to select an AO and partition it to a set of orbitals labeled "core," "valence", and "Rydberg," each of which contributes differently to the density. Core orbitals contribute exactly 2*e* to the atomic population, while the valence orbitals vary in their contributions and the Rydberg set participates minimally in the charges. In previous studies, our and other groups have highlighted the sensitivity of NPA charges to the initial partitioning of the NAO basis into valence and Rydberg sets. This is particularly true with regard to metals, where in the d block the default NPA partitioning of the NAOs excludes the formally empty set of p orbitals from the valence space of the metal atom. Including the 4p AO in the Rydberg set can lead to a larger positive charge on the metal than if it is considered part of the valence space, owing to the interaction between the empty p and the ligand orbitals.[62] The correct partitioning of the NAOs also influences predicted trends in atomic charges within a series. In our studies of 5f actinide complexes, we noted that the empty set of 6d orbitals (which may contribute to the bonding of the actinyls) is placed in the Rydberg basis and not in the valence. Altering the default partitioning scheme to have the 7s5f6d in the valence successfully reproduced trends in electron-donating capability within the equatorial ligands bound to UO_2^{2+}.[63]

Table 3. NPA Charges as a Function of Valence/Rydberg Partition of the NAO Basis[a] for $La(H_2O)_8^{3+}$ and $Lu(H_2O)_8^{3+}$ Using the Small-Core RECP and B3LYP/[9s8p5d4f3g]/aug-cc-pvdz

Valence/Rydberg partition	q_{Ln}
$La(H_2O)_8^{3+}$	
0/6–10s; 6–10p; 5–8d; 4–6f	2.846
6s/7–10s; 6–10p;5–8d; 4–6f	2.768
6s; 4f/7–10s; 6–10p; 5–8d; 5–6f	2.695
6s; 6p/7–10s; 7–10p; 5–8d; 4–f	2.542
6s; 6p; 5d/7–10s; 7–10p; 6–8d; 4–6f	2.032
6s; 6p; 5d; 4f/7–10s; 7–10p; 6–8d; 5–6f	1.948
$Lu(H_2O)_8^{3+}$	
0/6–11s; 6–10p; 5–8d; 5–7f	2.848
6s/7–11s; 6–10p; 5–8d; 5–7f	2.681
6s; 6p/7–11s; 7–10p; 5–8d; 5–7f	2.350
6s;5d/7–11s;7–10p;6–8d;5−7f	2.191
6s; 6p; 5d/7–11s; 7–10p; 6–8d; 5–7f	1.857

[a] The core NAOs of La(III) are the 4–5s; 4–5p; 4d and for Lu(III) are 4–5s; 4–5p; 4d; 4f. Default partitioning schemes are in bold.

In a similar vein, we have examined the appropriate NAOs to be placed in the valence space of trivalent La and Lu as well as the dependence of NPA charges upon the functional and basis set. This is particularly important as NPA has been extensively used to understand a variety of electronic effects including the influence of higher coordination numbers upon energetics of Ln(III) reactions and electronic structure.[9,64,65] The default partitioning for La(III) in $La(H_2O)_8^{3+}$ places the 4s and 5s, 4p and 5p, and 4d NAOs in the core; the 6s and the 4f in the valence; and the 7–10s, 6–10p, and 5f and 6f in the Rydberg space. To test the calculated metal charge as a function of the valence/Rydberg NAO partition, all valence NAOs were first placed in the Rydberg set and then systematically brought into the valence space (Table 3). In the case of zero NAOs participating in the valence set, the atomic charge on La(III) is quite near the formal charge of 3+ (q_{La} = 2.846). Inclusion of the 6s NAO in the valence space decreases the charge by 0.08*e*, and bringing in the 4f NAO adds another 0.07*e* to La(III). Thus, the charge on La(III) using the default NPA partitioning is 2.695. Similar contributions to the atomic charge are found with the 6p orbital in the valence; however, the largest effect is by far observed when the 5d NAO is allowed to participate in the valence. The 5d leads to an amazing 0.51*e* decrease in metal charge, clearly indicating its importance in the La(III) electronic structure. This result is not entirely unanticipated, as previous studies have noted the potential importance of the 5d orbitals, particularly as their energies are quite sensitive to the degree of relativistic effects.[6] Adding functions beyond the 6s6p5d4f has no substantial effect upon q_{La}, leading us to propose that these NAOs are the appropriate valence orbitals to calculate La(III) charges. This partitioning should also be appropriate for other Ln(III) cations, as going across the period constitutes filling the 4f shell.

Table 4. NPA Charges (q) Obtained with Different Density Functionals (at the Respective Optimized Geometries) Using Both the Modified (6s6p5d4f) and Default (6s4f for La(III) 6s5d for LuIII)) Valence Partition of the Small-Core RECP and the Segmented Contracted [9s8p5d4f3g] Basis

	modified valence		default valence	
	q_{La}	q_{Lu}	q_{La}	q_{Lu}
SVWN5	1.624	1.586	2.559	1.971
SPW92	1.623	1.586	2.558	1.971
PW91	1.821	1.766	2.622	2.107
PBE	1.863	1.771	2.650	2.111
TPSS	1.867	1.793	2.643	2.129
B3LYP	1.948	1.857	2.695	2.191
PBE0	1.925	1.867	2.689	2.205

In the case of $Lu(H_2O)_8^{3+}$, the default NPA partitioning places the 6s and 5d NAOs in the valence space, with the 4f in the core owing to the $4f^{14}$ electronic configuration. Similar results to those of $La(H_2O)_8^{3+}$ are obtained when the valence/Rydberg partitioning is modified; however, the relative contributions of the NAOs are somewhat altered (Table 3). As in $La(H_2O)_8^{3+}$, the metal charge is close to the formal charge of 3+ when all valence orbitals are placed in the Rydberg set. However, inclusion of the 6s in the valence partition decreases the atomic charge by 0.16e, nearly double that observed in La, and the 6p adds an additional 0.33e. The 5d adds 0.49e, which is slightly less than that found in $La(H_2O)_8^{3+}$. Including the 4f NAO in the valence space does not change q_{Lu} significantly, as it is doubly occupied and contributes exactly 2e when it is in the core space. The enhanced 6s and 6p contributions and decreased 5d participation in Lu(III) are in agreement with all electron DFT calculations of $La(H_2O)_{8,9}^{3+}$ and $Lu(H_2O)_{8,9}^{3+}$ using a zeroth-order regular approximation Hamiltonian, which indicates that the 5d orbitals are destabilized and the 6s orbitals are stabilized by increasing relativistic effects.[6] Since relativity plays an increasingly important role as one goes across the Ln period, the 6s orbital is more active in the metal−water interaction of $Lu(H_2O)_8^{3+}$ than in $La(H_2O)_8^{3+}$. However, the importance of the 6s is only manifested in the NPA and not within natural bond order analysis (NBO). Indeed, NBO predicts no covalent interaction between the Ln and ligating waters, irrespective of the partitioning of the valence space.

Using both the modified NPA and default partitioning schemes, the dependence of the metal charge upon basis set and density functional has also been examined. Table 4 shows the calculated charges on the metal center in $La(H_2O)_8^{3+}$ and $Lu(H_2O)_8^{3+}$ with different functionals at their respective optimized geometries. Both the modified and default NPA schemes predict that the metal charges increase as LSDA < GGA < meta-GGA < hybrid and that these charges span ~0.3e. Yet, the two partitions differ significantly when comparing q_{La} and q_{Lu}. Specifically, the default NPA charges predict that La(III) has nearly 0.5e less than Lu(III) in $Ln(H_2O)_8^{3+}$, while the modified NPA charges are within 0.1e for the two metals. This is an important observation if one is interested in calculating the relative surface charge density, ρ_s, of La(III) and Lu(III), as the default partition would significantly overemphasize the electrostatic differences across the Ln period.

Table 5. B3LYP NPA Charges (q) Using the Modified (6s6p5d4f) Valence Partition as a Function of Segmented Contracted Basis Set Using the Small-Core (ECP28MWB) RECP at the Optimized [9s8p5d4f3g] Geometry of $Ln(H_2O)_8^{3+}$ and Using the Large-Core (ECP47MWB in La and ECP60MWB in Lu) RECP at the Optimized Geometry

	q_{La}	q_{Lu}
	ECP28MWB	
[9s8p5d4f3g]	1.948	1.857
[9s8p5d3f]	2.035	1.900
[9s7p5d3f]	2.240	2.190
[9s6p5d3f]	2.442	2.315
[8s6p5d3f]	2.518	2.480
[7s6p5d3f]	2.573	2.552
[6s6p5d3f]	3.561	3.590
	ECP47MWB	ECP60MWB
[5s4p3d]	2.049	1.804

A comparison of the NPA charges as a function of basis set yields several important observations (Table 5). First, choice of the large-core or small-core RECP has little effect upon the calculated metal charge. Second, the calculated charges as a function of basis set truncation level qualitatively reflects the importance of key functions in the basis. For example, the g functions have neither energetic nor electrostatic importance, and truncation to the [6s6p5d3f] level yields completely unrealistic energies and charges for $Ln(H_2O)_8^{3+}$. In between these two extremes, NPA predicts roughly the same contributions of each function to the electrostatic description.

Conclusions

Benchmark calculations on $Ln(H_2O)_{1,8-9}^{3+}$ (Ln = La, Lu) have examined changes in predicted geometric and electronic structure using different density functionals and basis sets. Using the small-core RECP, we have highlighted specific functions for La^0 and Lu^0 that must be included in the basis for an adequate description of the Ln AOs. Using the (13s13p10d8f6g) uncontracted basis for La^{3+}, these are the 11th and 12th s functions and the ninth p function, while for Lu^{3+} the 10th through 12th s functions, the 12th p function, and the most diffuse f function are important. Differences in the calculated La^{3+} and Lu^{3+} HF and B3LYP cation densities have been identified as the source of a significant B3LYP contraction error in Lu^{3+}. As previously reported, large-core RECP calculations predict longer Ln−ligand bond lengths relative to small-core calculations. However, we have also shown that deviations in structural parameters extend beyond the Ln−ligand bonds and alter the H-bond distances in the primary hydration shell. In accordance with previous studies, we observe overbinding when using the LSDA functionals. The meta-GGA TPSS functional has the closest structural agreement of its optimized geometries relative to experimental results; however, the performance of the common B3LYP functional is also reasonable. Interestingly, LSDA, TPSS, and B3LYP calculate nearly identical lanthanide contraction values, while GGA, PBE, and PB0 have shorter values. In combination with our

basis set results, this highlights the misleading nature of the lanthanide contraction as a metric for assessing the quality of method/basis set combinations. In fact, Δ_{Ln} is remarkably insensitive to clear inadequacies of a basis due to cancellation of errors. Finally, we have examined the calculated charges from natural population analyses and proposed that the 6s6p5d4f NAOs be placed in the valence space when determining atomic charge. Clear deviations in the electrostatic description are observed when the NPA charges from the modified and default partitioning schemes are compared.

Acknowledgment. This work was sponsored by the U.S. Department of Energy, Office of Nuclear Energy, Science and Technology, Junior Faculty Award Program award #DE-FG07-05ID14692/IDNE006. This research was performed in part using (1) the Molecular Science Computing Facility (MSCF) in the William R. Wiley Environmental Molecular Sciences Laboratory, a national scientific user facility sponsored by the U.S. Department of Energy's Office of Biological and Environmental Research and located at the Pacific Northwest National Laboratory, operated for the Department of Energy by Battelle, and (2) the National Energy Research Scientific Computing Center (NERSC), a DOE Office of Science user facility at Lawrence Berkely National Laboratory. The author would also like to thank Prof. Kirk Peterson for several thoughtful discussions.

References

(1) Nielson, G. W.; Skipper, N. T. K^+ Coordination in Aqueous Solution. *Chem. Phys. Lett.* **1985**, *114*, 35–38.

(2) Neilson, G. W.; Broadbent, R. D. The Structure of Sr^{2+} in Solution. *Chem. Phys. Lett.* **1990**, *167*, 429–431.

(3) Salmon, P. S.; Neilson, G. W.; Enderby, J. E. The of Cu^{2+} Aqueous Solutions. *J. Phys. C.: Solid State Phys.* **1988**, *21*, 1335–1350.

(4) Choppin, G. R.; Rizkalla, E. N. Solution Chemistry of Actinides and Lanthanides. *Handb. Phys. Chem. Rare Earths* **1994**, *18*, 559–590.

(5) Kuchle, W.; Dolg, M.; Stoll, H. Ab Initio Study of the Lanthanide and Actinide Contraction. *J. Phys. Chem. A* **1997**, *101*, 7128–7133.

(6) Clavaguera, C.; Gognon, J. P.; Pyykko, P. Calculated Lanthanide Contractions for Molecular Trihalides and Fully Hydrated Ions: The Contributions from Relativity and 4f-shell Hybridization. *Chem. Phys. Lett.* **2006**, *429*, 8–12.

(7) Laerdahl, J. K.; Faegri, K., Jr.; Visscher, L.; Saue, T. A fully relativistic Dirac–Hartree–Fock and second-order Møller–Plesset study of the lanthanide and actinide contraction. *J. Chem. Phys.* **1998**, *109*, 10806–10816.

(8) Pyykko, P. Relativistic Effects in Structural Chemistry. *Chem. Rev.* **1988**, *88*, 563–594.

(9) Maron, L.; Eisenstein, O. Do f Electrons Play a Role in the Lanthanide-Ligand Bonds? A DFT Study of $Ln(NR_2)_3$; R = H, SiH_3. *J. Phys. Chem. A* **2000**, *104*, 7140–7143.

(10) Clark, D. L.; Gordon, J. C.; Hay, P. J.; Martin, R. L.; Poli, R. DFT Study of Tris(bis(trimethylsilyl)methyl)lanthanum and -samarium. *Organometallics* **2002**, *21*, 5000–5006.

(11) Reed, A. E.; Weinstock, R. B.; Weinhold, F. Natural Population Analysis. *J. Chem. Phys.* **1985**, *83*, 735–746.

(12) Slater, J. C. *Quantum Theory of Molecular and Solids*; McGraw-Hill: New York, 1974; Vol. 4: The Self-Consistent Field for Molecular and Solids.

(13) Hohenberg, P.; Kohn, W. Inhomogeneous Electron Gas. *Phys. Rev.* **1964**, *136*, B864–B871.

(14) Kohn, W.; Sham, L. J. Self-Consistent Equations Including Exchange and Correlation Effects. *Phys. Rev.* **1965**, *140*, A1133–A1138.

(15) Vosko, S. H.; Wilke, L.; Nusair, M. Accurate Spin-Dependent Electron Liquid Correlation Energies for Local Spin Density Calculations: A Critical Analysis. *Can. J. Phys.* **1980**, *58*, 1200–1211.

(16) Perdew, J. P.; Wang, Y. Accurate and Simple Analytic Representation of the Electron-Gas Correlation Energy. *Phys. Rev. B: Condens. Matter Mater. Phys.* **1992**, *45*, 13244–13249.

(17) Perdew, J. P.; Burke, K.; Ernzerhof, M. Generalized Gradient Approximation Made Simple. *Phys. Rev. Lett.* **1996**, *77*, 3865–3868.

(18) Becke, A. D. Density-Functional Exchange-Energy Approximation with Correct Asymptotic Behavior. *Phys. Rev. A: At., Mol., Opt. Phys.* **1988**, *38*, 3098.

(19) Perdew, J. P. Density-Functional Approximation for the Correlation Energy of the Inhomogeneous Electron Gas. *Phys. Rev. B: Condens. Matter Mater. Phys.* **1986**, *33*, 8822.

(20) Perdew, J. P. *Electronic Structure of Solids*; Ziesche, P., Eschrig, H., Eds.; Akademie: Berlin, 1991.

(21) Burke, K.; Perdew, J. P.; Wang, Y. *Electronic Density Functional Theory: Recent Progress and New Directions*; Dobson, J. F., Vignale, G., Das, M. P., Eds.; Plenum Press: New York, 1998.

(22) Perdew, J. P.; Chevary, J. A.; Vosko, S. H.; Jackson, K. A.; Pederson, M. R.; Singh, D. J.; Fiolhais, C. Atoms, Molecules, Solids, and Surfaces: Applications of the Generalized Gradient Approximation for Exchange and Correlation. *Phys. Rev. B: Condens. Matter Mater. Phys.* **1992**, *46*, 6671–6687; **1993**, *48*, 4978(E).

(23) Becke, A. D. Density-functional Thermochemistry. III. The Role of Exact Exchange. *J. Chem. Phys.* **1993**, *98*, 5648–5652.

(24) Lee, C.; Yang, W.; Parr, R. G. Development of the Colle-Salvetti Correlation-Energy Formula into a Functional of the Electron Density. *Phys. Rev. B: Condens. Matter Mater. Phys.* **1988**, *37*, 785–789.

(25) (a) Stephens, P. J.; Devlin, F. J.; Chabalowski, C. F.; Frisch, M. J. Ab Initio Calculation of Vibrational Absorption and Circular Dichroism Spectra Using Density Functional Force Fields. *J. Phys. Chem.* **1994**, *98*, 11623–11627. (b) Hertwig, R. H.; Koch, W. On the Parameterization of the Local Correlation Functional. What is Becke-3-LYP? *Chem. Phys. Lett.* **1997**, *268*, 345.

(26) Ernzerhof, M.; Scuseria, G. E. Assessment of the Perdew–Burke–Ernzerhof Exchange-Correlation Functional. *J. Chem. Phys.* **1999**, *110*, 5029–5036.

(27) Tao, J.; Perdew, J. P.; Staroverov, V. N.; Scuseria, G. E. Climbing the Density Functional Ladder: Nonempirical Meta-Generalized Gradient Approximation Designed for Molecules and Solid. *Phys. Rev. Lett.* **2003**, *91*, 146401–146405.

(28) Bylaska, E. J.; de Jong, W. A.; Kowalski, K.; Straatsma, T. P.; Valiev, M.; Wang, D.; Aprà, E.; Windus, T. L.; Hirata, S.; Hackler, M. T.; Zhao, Y.; Fan, P.-D.; Harrison, R. J.; Dupuis, M.; Smith, D. M. A.; Nieplocha, J.;

Tipparaju, V.; Krishnan, M.; Auer, A. A.; Nooijen, M.; Brown, E.; Cisneros, G.; Fann, G. I.; Früchtl, H.; Garza, J.; Hirao, K.; Kendall, R.; Nichols, J. A.; Tsemekhman, K.; Wolinski, K.; Anchell, J.; Bernholdt, D.; Borowski, P.; Clark, T.; Clerc, D.; Dachsel, H.; Deegan, M.; Dyall, K.; Elwood, D.; Glendening, E.; Gutowski, M.; Hess, A.; Jaffe, J.; Johnson, B.; Ju, J.; Kobayashi, R.; Kutteh, R.; Lin, Z.; Littlefield, R.; Long, X.; Meng, B.; Nakajima, T.; Niu, S.; Pollack, L.; Rosing, M.; Sandrone, G.; Stave, M.; Taylor, H.; Thomas, G.; van Lenthe, J.; Wong, A.; Zhang, Z. *NWChem, A Computational Chemistry Package for Parallel Computers*, Version 5.0; Pacific Northwest National Laboratory: Richland, WA, 2006.

(29) Frisch, M. J.; Trucks, G. W.; Schlegel, H. B.; Scuseria, G. E.; Robb, M. A.; Cheeseman, J. R.; Montgomery, J. A., Jr.; Vreven, T.; Kudin, K. N.; Burant, J. C.; Millam, J. M.; Iyengar, S. S.; Tomasi, J.; Barone, V.; Mennucci, B.; Cossi, M.; Scalmani, G.; Rega, N.; Petersson, G. A.; Nakatsuji, H.; Hada, M.; Ehara, M.; Toyota, K.; Fukuda, R.; Hasegawa, J.; Ishida, M.; Nakajima, T.; Honda, Y.; Kitao, O.; Nakai, H.; Klene, M.; Li, X.; Knox, J. E.; Hratchian, H. P.; Cross, J. B.; Bakken, V.; Adamo, C.; Jaramillo, J.; Gomperts, R.; Stratmann, R. E.; Yazyev, O.; Austin, A. J.; Cammi, R.; Pomelli, C.; Ochterski, J. W.; Ayala, P. Y.; Morokuma, K.; Voth, G. A.; Salvador, P.; Dannenberg, J. J.; Zakrzewski, V. G.; Dapprich, S.; Daniels, A. D.; Strain, M. C.; Farkas, O.; Malick, D. K.; Rabuck, A. D.; Raghavachari, K.; Foresman, J. B.; Ortiz, J. V.; Cui, Q.; Baboul, A. G.; Clifford, S.; Cioslowski, J.; Stefanov, B. B.; Liu, G.; Liashenko, A.; Piskorz, P.; Komaromi, I.; Martin, R. L.; Fox, D. J.; Keith, T.; Al-Laham, M. A.; Peng, C. Y.; Nanayakkara, A.; Challacombe, M.; Gill, P. M. W.; Johnson, B.; Chen, W.; Wong, M. W.; Gonzalez, C.; Pople, J. A. *Gaussian 03*, Revision C.02; Gaussian, Inc.: Wallingford, CT, 2004.

(30) Cao, X.; Dolg, M. Valence Basis Sets for Relativistic Energy-Consistent Small-Core Lanthanide Pseudopotentials. *J. Chem. Phys.* **2001**, *115*, 7348–7355.

(31) Cao, X.; Dolg, M. Segmented Contraction Scheme for Small-Core Lanthanide Pseudopotential Basis Sets. *THEOCHEM* **2002**, *581*, 139.

(32) Dolg, M.; Stoll, H.; Savin, A.; Preuss, H. Pseudopotential Study of the Rare Earth Monohydrides, Monoxides, and Monofluorides. *Theor. Chim. Acta* **1989**, *75*, 173–194.

(33) (a) Dunning, T. H., Jr. Gaussian Basis Sets for Use in Correlated Molecular Calculations. I. The Atoms Boron through Neon and Hydrogen. *J. Chem. Phys.* **1989**, *90*, 1007–1023. (b) Kendall, R. A.; Dunning, T. H., Jr.; Harrison, R. J. Electron Affinities of the First-Row Atoms Revisited. Systematic Basis Sets and Wave Functions. *J. Chem. Phys.* **1992**, *96*, 6796–6806.

(34) Mulliken, R. S. Electronic Population Analysis on LCAOMO Molecular Wave Functions. I. *J. Chem. Phys.* **1955**, *23*, 1833–1840.

(35) Shannon, R. D. Revised Effective Ionic Radii and Systematic Studies of Interatomic Distances in Halides and Chalcogenides. *Acta Crystallogr., Sect. A* **1976**, *32*, 751–767.

(36) Quadrelli, E. A. Lanthanide Contraction over the 4f Serie Followsa Quadratic Decay. *Inorg. Chem.* **2002**, *41*, 167–169.

(37) Seitz, M.; Oliver, A. G.; Raymond, K. N. The Lanthanide Contraction Revisited. *J. Am. Chem. Soc.* **2007**, *129*, 11153–11160.

(38) Deng, B.; Ellis, D. E.; Ibers, J. A. New Layered Rubidium Rare-Earth Selenides: Syntheses, Structures, Physical Properties, and Electronic Structures for $RbLnSe_2$. *Inorg. Chem.* **2002**, *41*, 5716–5720.

(39) Yao, J.; Deng, B.; Sherry, L. J.; McFarland, A. D.; Ellis, D. E.; Van Duyne, R. P.; Ibers, J. A. Syntheses, Structure, Some Band Gaps, and Electronic Structures of $CsLnZnTe_3$ (Ln = La, Pr, Nd, Sm, Gd, Tb, Dy, Ho, Er, Tm, Y). *Inorg. Chem.* **2004**, *43*, 7735–7740.

(40) Baisch, U.; Belli Dell'Amico, D.; Calderazzo, F.; Conti, R.; Labella, L.; Marchetti, F.; Quadrelli, E. A. The Mononuclear and Dinuclear Dimethoxyethane Adducts of Lanthanide Trichlorides $[LnCl_3(DME)_2)_n$, $n = 1$ or 2, Fundamental Starting Materials in Lanthanide Chemistry: Preparations and Structures. *Inorg. Chim. Acta* **2004**, *357*, 1538–1548.

(41) Baisch, U.; Belli Dell'Amico, D.; Calderazzo, F.; Labella, L.; Marchetti, F.; Merigo, A. N,N-Dialkylcarbamato Lanthanide Complexes, a series of Isotypical Coordination Compounds. *Eur. J. Inorg. Chem.* **2004**, 1219.

(42) Slater, J. C. Atomic Shielding Constants. *Phys. Rev.* **1930**, *36*, 57–64.

(43) Clementi, E.; Raimondi, D. L. Atomic Screening Constants from SCF Functions. *J. Chem. Phys.* **1963**, *38*, 2686–2689.

(44) Clementi, E.; Raimondi, D. L.; Reinhardt, W. P. Atomic Screening Constants from SCF Functions. II. Atoms with 37 to 86 Electrons. *J. Chem. Phys.* **1967**, *47*, 1300–1307.

(45) Pyykko, P. Dirac-Fock One Centre Calculations Part 8. The 1Σ States of ScH, YH, LaH, AcH, TmH, LuH and LrH. *Phys. Scr.* **1979**, *20*, 647–651.

(46) Schwarz, W. H. E. Relativistic calculations of molecules relativity and bond lengths. *Phys. Scr.* **1987**, *36*, 403–411.

(47) Habenschuss, A.; Spedding, F. H. The coordination (hydration) of rare earth ions in aqueous chloride solutions from X-Ray diffraction. I. $TbCl_3$, $DyCl_3$, $ErCl_3$, $TmCl_3$, and $LuCl_3$. *J. Chem. Phys.* **1979**, *70*, 2797–2806.

(48) Habenschuss, A.; Spedding, F. H. The coordination (hydration) of rare earth ions in aqueous chloride solutions from x-ray diffraction. II. $LaCl_3$, $PrCl_3$, and $NdCl_3$. *J. Chem. Phys.* **1979**, *70*, 3758–3763.

(49) Yamauchi, S.; Kanno, H.; Akama, Y. Far-Infrared Evidence for the Hydration Number Change of Rare Earth Ions in Aqueous Solution. *Chem. Phys. Lett.* **1988**, *151*, 315–317.

(50) Mochizuki, Y.; Tatewaki, H. *Chem. Phys.* **2001**, *273*, 135–148.

(51) Clark, A. E.; Martin, R. L.; Hay, P. J.; Green, J. C.; Jantunen, K. C.; Kiplinger, J. L. Electronic structure, excited states, and photoelectron spectra of uranium, thorium, and zirconium bis(ketimido) complexes $(C_5R_5)_2M[-N{=}CPh_2]_2$ (M = Th, U, Zr; R = H, CH_3). *J. Phys. Chem. A* **2005**, *109*, 5481–5491.

(52) Peralta, J. E.; Batista, E. R.; Scuseria, G. E.; Martin, R. L. All-Electron Hybrid Density Functional Calculations on UF_n and UCl_n ($n = 1$–6). *J. Chem. Theory Comput.* **2005**, *1*, 612–616.

(53) Perdew, J. P.; Schmidt, K. *Density Functional Theory and Its Application to Materials*; Van Doren, E., Ed.; AIP Press: Melville, NY, 2001.

(54) Vetere, V.; Maldivi, P.; Adamo, C. Comparative studies of quasi-relativistic density functional methods for the description

of lanthanide and actinide complexes. *J. Comput. Chem.* **2003**, *24*, 850.

(55) Adamo, C.; Maldivi, P. A Theoretical Study of Bonding in Lanthanide Trihalides by Density Functional Methods. *J. Phys. Chem. A* **1998**, *102*, 6812–6820.

(56) Petit, L.; Borel, A.; Daul, C.; Maldivi, P.; Adamo, C. A Theoretical Characterization of Covalency in Rare Earth Complexes through Their Absorption Electronic Properties: f-f Transitions. *Inorg. Chem.* **2006**, *45*, 7382–7388.

(57) Gutowski, K. E.; Dixon, D. A. Predicting the Energy of the Water Exchange Reaction and Free Energy of Solvation for the Uranyl Ion in Aqueous Solution. *J. Phys. Chem. A* **2006**, *110*, 8840–8856.

(58) Cundari, T. R.; Stevens, W. J. Effective Core Potential Methods for Lanthanides. *J. Chem. Phys.* **1993**, *98*, 5555–5565.

(59) Stevens, W. J.; Krauss, M.; Basch, H.; Jasien, P. G. Relativistic Compact Effective Potentials and Efficient, Shared-Exponent Basis Sets for the Third-, Fourth-, and Fifth-Row Atoms. *Can. J. Chem.* **1992**, *70*, 612–630.

(60) Dinescu, A.; Clark, A. E. Thermodynamic and Structural Features of Aqueous Ce(III). *J. Phys. Chem. A*, in preparation.

(61) (a) Löwdin, P.-O. On the Non-Orthogonality Problem Connected with the Use of Atomic Wave Functions in the Theory of Molecules and Crystals. *J. Chem. Phys.* **1950**, *18*, 365. (b) Löwdin, P.-O. On the Non-Orthogonality Problem. *Adv. Quantum Chem.* **1970**, *5*, 185.

(62) Maseras, F.; Morokuma, K. Application of the natural population analysis to transition-metal complexes. Should the empty metal p orbitals be included in the valence space. *Chem. Phys. Lett.* **1992**, *195*, 500–504.

(63) Clark, A. E.; Sonnenberg, J.; Hay, P. J.; Martin, R. L. Density and wave function analysis of actinide complexes: What can fuzzy atom, atoms-in-molecules, Mulliken, Löwdin, and natural population analysis tell us. *J. Chem. Phys.* **2004**, *121*, 2563–2570.

(64) Dobler, M.; Guilbaud, P.; Dedieu, A.; Wipff, G. Interaction of Trivalent Lanthanide Cations with Nitrate Anions: A Quantum Chemical Investigation of Monodentate/Bidentate Binding Modes. *New J. Chem.* **2001**, *25*, 1458–1465.

(65) Saloni, J.; Roszak, S.; Hilpert, K.; Popovic, A.; Miller, M.; Leszczynski, J. Mass Spectrometric and Quantum Chemical Studies of the Thermodynamics and Bonding of Neutral and Ionized LnCl, $LnCl_2$, and $LnCl_3$ Species (Ln = Ce, Lu). *Inorg. Chem.* **2006**, *45*, 4508–4517.

CT700317P